

# Turbulent flows for relativistic conformal fluids in 2+1 dimensions

Federico Carrasco<sup>1,2</sup>, Luis Lehner<sup>2,3</sup>, Robert C. Myers<sup>2</sup>,  
Oscar Reula<sup>1</sup>, Ajay Singh<sup>2,4</sup>

<sup>1</sup>*FaMAF-UNC, IFEG-CONICET, Ciudad Universitaria, 5000, Cordoba, Argentina.*

<sup>2</sup>*Perimeter Institute for Theoretical Physics, Waterloo, Ontario N2L 2Y5, Canada.*

<sup>3</sup>*Department of Physics, University of Guelph, Guelph, Ontario N1G 2W1, Canada.*

<sup>4</sup>*Department of Physics & Astronomy and Guelph-Waterloo Physics Institute,  
University of Waterloo, Waterloo, Ontario N2L 3G1, Canada*

We demonstrate that relativistic conformal hydrodynamics in 2+1 dimensions displays a turbulent behaviour which cascades energy to longer wavelengths on both flat and spherical manifolds. Our motivation for this study is to understand the implications for gravitational solutions through the AdS/CFT correspondence. The observed behaviour implies gravitational perturbations of the corresponding black brane/black hole spacetimes (for sufficiently large scales/temperatures) will display a similar cascade towards longer wavelengths.

## I. INTRODUCTION

The AdS/CFT correspondence [1, 2] provides a remarkable framework for studying certain strongly coupled gauge theories in  $d$  dimensions by mapping to weakly coupled gravitational systems in  $d + 1$  dimensions. Of particular interest is the relation between gauge theory plasmas and black hole geometries [3–5]. Here the correspondence was used to show that perturbed black brane geometries at the classical level have a dual description in terms of fluid dynamics equations governing long-wavelength perturbations about an equilibrium state. This fluid/gravity correspondence builds on the highly successful and ongoing program to calculate the near-equilibrium transport coefficients for strongly coupled plasmas using holographic techniques, e.g., [6, 7].

This duality has been exploited in a large number of works which exploit known gravitational behaviour to infer properties of diverse systems described by strongly coupled field theories in the large  $N$  limit. On the hydrodynamical front, work in [8] describes how the onset of naked singularities can be tied to finite-time blowups in hydrodynamics. Additionally, numerical simulations are increasingly being exploited to understand isotropization and thermalization of systems starting far from equilibrium, e.g., [9–15].

In all these works, the approach has been to understand the behaviour of relevant systems in the gravitational side of the duality and infer from it properties of the gauge theory dynamics. In the present work, we follow the opposite route, namely to study particular phenomena that might arise in the field theory to understand possibly unexpected phenomena on the gravitational side.

Our starting point is a simple and well-known observation about the behaviour of turbulence of Newtonian fluids in two spatial dimensions. Specifically in this case, turbulent behaviour induces an energy cascade from short to long wavelengths e.g., [16]. This contrasts to the standard cascade from long to short scales characterizing turbulence in three and higher dimensions.[54]

The obvious question is therefore whether this effect appears in the relativistic conformal fluids relevant for the AdS/CFT correspondence, and if so, what is the dual interpretation in the gravitational theory. A positive answer would seem to distinguish AdS gravity in four dimensions from higher dimensions in a unique way. An affirmative answer is also particularly intriguing as the two known instabilities in AdS spacetimes, super-radiance and the recently found ‘mildly-turbulent’ behaviour in [17], both induce energy cascades from low to high frequencies for all  $d \geq 3$ .

To answer this question, which has also been raised earlier[5], we examine the behaviour of specific fluid flows which are dual to perturbations of Schwarzschild and Kerr black holes in  $AdS_4$ . We study the problem for spherical horizons in global coordinates, as well as planar horizons described by Poincaré coordinates. Specifically, we study the relativistic Euler equations with the particular equation of state corresponding to a conformal fluid on a fixed  $\mathfrak{R} \times S^2$  manifold for the former case while  $\mathfrak{R} \times T^2$  for the latter. In each background, we examine perturbations of the stationary configurations dual to the corresponding stationary black holes. We then examine the onset of turbulence and its cascade behaviour in this setup, and compare it with the expected behaviour for the case of incompressible non-relativistic flows with ‘standard’ equations of state. We find that, as in the Newtonian case, turbulence leads to perturbations cascading from shorter to longer wavelengths for relativistic conformal hydrodynamics in 2+1 dimensions.

This work is organized as follows: in the remainder of this section we briefly review some well known aspects about turbulence in two and three spatial dimensions. Section II discusses the initial configurations considered, as well as details of our numerical implementation. Section III presents results for the cases considered for conformal hydrodynamics on the sphere (the results on the torus, which are qualitatively similar, are included in an appendix). We discuss the consequences of the obtained behaviour in section IV. (Visualizations of the fluid flows studied here can be found in [18]).

## A. Turbulence

Turbulence is a ubiquitous property of fluid flows observed in nature [19]. Qualitatively, we might describe turbulence as a flow regime characterized by chaotic or stochastic behaviour. Most of our theoretical understanding of turbulence comes from the study of non-relativistic incompressible fluids. Certainly, while a full understanding of turbulence is not yet available, some robust results do exist. Namely, for the inviscid case in two spatial dimensions, a global regularity theorem has been proved, together with theorems about uniqueness and existence of solutions [20] implying no singularity of the velocity field can develop in a finite time.

For the three-dimensional case it is not yet known whether the same holds true and resolving this issue constitutes a major open problem (see e.g., [21]). It is known however, that qualitatively two and three dimensional turbulent fluid flows exhibit profound differences arising from the existence of a key conserved quantity which has a radical effect in the fluid's turbulent behaviour. This quantity, dubbed *enstrophy*, — see discussion around (18) — has been argued to imply a very different cascade picture in two dimensions, as compared to the three-dimensional one [22]. Small scales will support a ‘*direct enstrophy cascade*’ towards smaller wavelengths, with all the enstrophy dissipation taking place on the shortest scales. The energy flux towards small scales will then be damped and the energy will be, instead, transferred to larger scales in an ‘*inverse energy cascade*’. This behaviour is observed in nature, controlled experiments and numerical simulations.

In a phenomenological theory of two-dimensional turbulence [22, 23], the existence of two inertial ranges was pointed out: a direct  $k^{-3}$  enstrophy cascade at small wavelengths, and an inverse energy cascade with spectrum  $k^{-5/3}$ , at larger scales, were predicted.

Numerical simulations have shown the emergence of strong coherent vortex structures that dominates the flow after some time [24]. These vortices emerge as anomalous fluctuations at small scales, and have a lifetime much longer than their characteristic eddy turnover time [25]. As the dynamics continues, two such vortices might collide and usually merge if they rotate in the same direction, forming a vortex of larger scale. In the process the energy is nearly conserved, so it acts as the mechanism of inverse energy cascade. The statistical distribution of vortices over scales leads to an energy spectrum  $k^{-3}$  which is much steeper than the originally expected  $k^{-5/3}$ , and vortices were recognized as the fluctuations responsible of *intermittency* and possible anomalous dimensions [26].

The emergence and dynamics of vortices still pose a number of difficult questions, and the relevance of the initial data and external forcing is not yet fully understood. An exciting possibility, of course, would be that holographic studies might shed new light on this problem from a fundamentally different point of view.

## II. EQUATIONS, RATIONALE AND NUMERICAL IMPLEMENTATION

Our goal is to study the dynamics dual to a perturbed black hole in  $3 + 1$  dimensions from the global point of view, so we consider the field theory in  $2 + 1$  dimensions on the sphere (or a torus, see Appendix A). To do so, and in order to deal with a well posed problem, we restrict to the zeroth order expansion of the theory, i.e., to the equations determined by the conservation of the stress energy tensor of a perfect fluid. One reason for this choice is that the inclusion of viscous terms would yield an acausal system of equations [27–30] (for a recent discussion in the holographic context see e.g., [31]).[55] Hence properly incorporating these effects poses a serious complication for the corresponding simulations.

At first sight, working with perfect fluid equations would seem to be a severe limitation for our study and the conclusions that can be drawn from this work. However, recall that hydrodynamics treats the conservation of a stress-energy tensor in a gradient expansion, e.g., [32, 33]. For the conformal case, no intrinsic scales appear in defining the fluid and hence the temperature naturally controls the equation of state and all of the non-vanishing transport parameters. Hence to the stress tensor for a conformal fluid, in  $d$  spacetime dimensions, takes the following form

$$T_{\mu\nu} = \alpha T^d \left( (g_{\mu\nu} + d u_\mu u_\nu) - \frac{d\beta}{T} \sigma_{\mu\nu} + \mathcal{O}(T^{-2}) \right) \quad (1)$$

where  $\sigma_{ab}$  describes the first-order viscous contribution and  $\alpha, \beta$  are dimensionless coefficients which characterize the fluid. From this expression, we see that the viscous terms can be arbitrarily suppressed by increasing the temperature. To be more precise, if the characteristic scales  $L$  controlling the flow are kept fixed, i.e., the size of the sphere (or torus) in the present case, the gradient expansion becomes an expansion in  $1/LT$  and the higher order terms are suppressed by setting  $LT \gg 1$ . Thus the perfect fluid can be seen as an arbitrarily good approximation in this regime. Further, as we discussed above, turbulence is expected to generate a cascade from short to long scales for fluids in two spatial dimensions. In fact, our simulations will confirm this expectation and so the interesting dynamics here indeed progresses mainly towards longer and longer scales. Hence the viscous and higher order terms should not play a significant role in the observed behaviour.

To further support the conclusion that the viscous contributions are insignificant, we will consider two ways of incorporating effects of these terms: (i) through the addition of an artificial viscosity (as defined in [34, 35]) and (ii) by comparing results for higher temperatures, where the viscous and higher terms become less relevant (as described above), and showing that the observed turbulent behaviour remains unchanged both qualitatively and quantitatively, e.g., see figure 5. Notice that one could add terms up to second order in the derivative ex-

pansion (third order in derivatives) as suggested in [32] (which provides a modern extension of the method suggested in [28]). This approach effectively amounts to controlling and reducing gradients in the solution through a dynamical equation governing second order gradients of the flow. As we will see, the natural evolution of the system to longer wavelengths renders these approaches unnecessary.

In what follows we describe the system of equations considered, discuss useful monitoring quantities — including the conserved quantity associated to the enstrophy — as well as a brief summary of stationary solutions inferred from the dual gravitational picture.

### A. Evolution Equations

The system follows from the local conservation of the stress-energy tensor of a perfect fluid,

$$T^{\mu\nu} = (\rho + p) u^\mu u^\nu + p g^{\mu\nu}, \quad (2)$$

along with the condition of conformal invariance that requires the stress tensor to be traceless, i.e.,  $T^\mu_\mu = 0$ . This latter condition fixes the equation of state as

$$p = \rho/2, \quad (3)$$

for a conformal fluid in 2+1 dimensions — compare with (1) for general dimensions.

The set of dynamical variables we have chosen to evolve the system are:  $\{\tilde{\rho}, u_i\}$ , where  $\tilde{\rho} \equiv \log(\rho^{1/3})$ . The remaining component of the three-velocity,  $u^0$ , which can be identified with the Lorentz factor  $\gamma$  ( $u^0 \equiv \gamma = (1 - v^2)^{-1/2}$ ), is obtained at each time-step through the normalization condition  $u_\mu u^\mu = -1$ . In equilibrium, the temperature  $T$  of the system is related with the above variables by  $\rho = T^3$ , or equivalently,  $T = e^{\tilde{\rho}}$ . [56]

The system of evolution equations obtained for our dynamical variables then reads,

$$\partial_t \tilde{\rho} = \frac{1}{\alpha\gamma} \left\{ z\mathcal{D}\tilde{\rho} + z\vartheta - \frac{1}{2}\mathcal{D}z \right\}, \quad (4)$$

$$\partial_t u_i = \frac{1}{\alpha\gamma} \left\{ [\alpha\partial_i + u_i\mathcal{D}] \tilde{\rho} + \alpha\mathcal{D}u_i - zu_i\vartheta + \frac{u_i}{2}\mathcal{D}z \right\} \quad (5)$$

The spatial derivatives along the flow are denoted by  $\mathcal{D} \equiv u^k D_k$ , while  $\vartheta \equiv D_k u^k$  is the spatial divergence and  $D_k$  is the covariant derivative associated with the spatial metric  $h_{ij}$ . We also have defined,  $z \equiv \gamma^2$  and  $\alpha \equiv 1 + \gamma^2$ .

### B. Equilibrium Configurations

Equilibrium configurations for the toroidal case are simply constant temperature/constant velocity fluid flows and we adopt conditions as described in the appendix. The equilibrium states for conformal fluids on

the two-sphere can be obtained straightforwardly by requiring no entropy production within the first sub-leading (dissipative) order in the fluid expansion at equilibrium. This imposes a restrictive condition for the shear viscosity (i.e.,  $\sigma_{ab} = 0$ ). A simple family of such configurations corresponds to rigidly rotating fluids, which in our variables are given by

$$u^\theta = 0, \quad u^\phi = \gamma\omega_0, \quad T = \gamma\tau \quad (6)$$

where  $\gamma = (1 - \omega_0^2 \sin^2(\theta))^{-1/2}$  is the Lorentz factor. The two (constant) parameters characterizing these solutions are: the  $\omega_0$ , the angular rotation rate, and  $\tau$ , the local temperature measured by co-moving observers. Note that implicitly, we have set the radius of the  $S^2$  to one here, i.e., the proper length of the equator,  $\theta = \pi/2$ , is simply  $2\pi$ .

The thermodynamics and the local stress tensor of these solutions has been found to be in precise agreement with thermodynamics and boundary stress tensor of the spinning black holes [36]. In this reference, the authors compare conformal fluids on spheres of arbitrary dimensions with large rotating black holes on  $AdS$  spaces. First, global thermodynamical quantities are compared. Then, appealing to the duality, a comparison is made between the local stress tensor of the fluid configuration and the boundary stress tensor for the most general rotating black hole in  $AdS_{d+1}$ , as given in [37]. The relevant black hole solution for our case, the one corresponding to Kerr  $AdS_4$ , is labeled by two parameters  $a$  and  $r_+$ , related with the angular momentum (per unit mass) and the horizon radius of the black hole, respectively. Perfect agreement was found between these two theories in the large  $r_+$  limit, upon the following identifications [36]:

$$\omega_0 \longleftrightarrow a, \quad (7)$$

$$\tau \longleftrightarrow \frac{3r_+}{4\pi}. \quad (8)$$

Thus, the static configuration with  $\omega_0 = 0$  is the fluid dual to  $AdS_4$  Schwarzschild black hole, and the rotating fluid configurations ( $\omega_0 \neq 0$ ) are dual to the  $AdS_4$  Kerr geometry.

### C. Conservation Laws

Conserved quantities are invaluable tools to analyze the behaviour of any given system and, as discussed, their existence can imply a particular behaviour of the fluid flow. We here discuss these quantities which we monitor in our efforts to understand the behaviour of the system, in particular the phenomenon of turbulence. In particular, given a conserved current  $J^\mu$  (i.e.,  $\nabla_\mu J^\mu = 0$ ), the existence of a conserved charge immediately follows,

$$\int_{S^2} J^0 d\Sigma = const. \quad (9)$$

Hence in the following, we identify various conserved currents and charges for the present system.

Given a killing vector field  $K_\mu$  and the conserved stress tensor, the current  $J^\mu \equiv T^{\mu\nu}K_\nu$ , is automatically conserved. Thus, from the killing vectors,  $\xi \sim \frac{\partial}{\partial t}$  and  $\zeta \sim \frac{\partial}{\partial \phi}$ , we construct the first two conserved quantities that are identified with the total **energy** and **angular momentum** of the fluid, respectively:

$$E \equiv \frac{1}{2} \int_{S^2} \rho(3\gamma^2 - 1) d\Sigma, \quad (10)$$

$$L_\phi \equiv \frac{3}{2} \int_{S^2} \rho \gamma u^\phi d\Sigma. \quad (11)$$

From thermodynamical considerations, one knows that the local entropy  $s \equiv \rho^{2/3}$ , is conserved along the flow direction (in a perfect fluid). Thus, the current  $J^\mu = su^\mu$  is conserved and total **entropy** conservation follows,

$$S \equiv \int_{S^2} \rho^{2/3} \gamma d\Sigma. \quad (12)$$

Another quantity of interest is the **vorticity** which arises as a purely geometric property (i.e., independent of the equations of motion). It is constructed by taking the exterior derivative to the flow velocity, resulting in the vorticity two-form  $\omega_{\mu\nu} \equiv \partial_{[\mu} u_{\nu]}$ . In 2+1 dimensions, one can define a naturally conserved current just by taking its Hodge dual, i.e., we define  $W^\alpha = \epsilon^{\alpha\mu\nu} \omega_{\mu\nu}$ . The total ‘circulation’, which remains constant throughout the evolution, is then

$$C \equiv \int_{S^2} W^0 d\Sigma = \int_{S^2} \epsilon^{0ij} \omega_{ij} d\Sigma. \quad (13)$$

However, note that the conservation law is ‘topological’ in this case and so this conserved charge actually vanishes since  $C = - \int_{S^2} \mathbf{d}\mathbf{u} = 0$ .

Finally, we define the **enstrophy**, whose conservation plays a crucial role on two-dimensional turbulence and its *inverse cascade* scenario. This quantity, for incompressible non-relativistic fluids, is just the integral of the square vorticity field. Carter [38] has generalized the concept for relativistic fluids in three spatial dimensions, and we extend it here for two-dimensional relativistic conformal fluids.

Let us begin with  $\nabla_\mu T^{\mu\nu} = 0$  with the stress tensor given in (2) for a conformal fluid in  $d$  spacetime dimensions (i.e.,  $p = \rho/(d-1)$ ). For convenience we project these conservation equations along and orthogonal to the flow velocity,

$$u^\mu \partial_\mu \rho = -\frac{d}{d-1} \rho (\nabla_\mu u^\mu) \equiv -\frac{d}{d-1} \rho \Theta, \quad (14)$$

$$P^{\mu\nu} \partial_\nu \rho = -d\rho u^\nu \nabla_\nu u^\mu \equiv -d\rho a^\mu; \quad (15)$$

where  $\Theta$  is the (full covariant) divergence;  $a^\mu$ , the acceleration; and  $P^{\mu\nu} \equiv g^{\mu\nu} + u^\mu u^\nu$ , the projector perpendicular to  $u^\mu$ . Next, consider the two-form,

$$\Omega_{\mu\nu} = \nabla_{[\mu} \rho^{1/d} u_{\nu]}, \quad (16)$$

which is built to satisfy the *Carter-Lichnerowicz equation of motion*

$$\Omega_{\mu\nu} u^\nu = 0, \quad (17)$$

which is equivalent to (15). Note that the inclusion of  $\rho^{1/d}$  in (16) is crucial to produce this formulation of the equations of motion. Then, from the *Cartan Identity*, is straightforward to show that

$$\mathcal{L}_{\lambda\mathbf{u}} \Omega = \lambda \mathbf{u} \cdot \mathbf{d}\Omega + \mathbf{d}(\lambda \mathbf{u} \cdot \Omega) = 0. \quad (18)$$

Here the first term vanishes because  $\Omega = \mathbf{d}(\rho^{1/d} \mathbf{u})$  is an exact form, while the second term vanishes by the Carter-Lichnerowicz equation (17). This means that the two-form  $\Omega$  does not change along the flow direction.

The latter observation motivates one to look for a new conservation law, however, we will only be able to construct the desired result by using an identity which only holds for  $d = 3$ , i.e., two spatial dimensions. In this case, we write the following current:  $J^\mu \equiv \rho^{-2/3} (\Omega^{\alpha\beta} \Omega_{\alpha\beta}) u^\mu$ . To establish that this current is conserved, we make use of the identity,

$$\Omega^{\mu\alpha} \Omega_{\mu\beta} = \frac{1}{2} \Omega^2 P_\beta^\alpha, \quad (19)$$

where  $\Omega^2 \equiv \Omega_{\mu\nu} \Omega^{\mu\nu}$ . The latter holds for two spatial dimensions since we can write,  $\Omega_{\mu\nu} = \epsilon_{\mu\nu\alpha} l^\alpha$ , for some arbitrary vector  $l^\alpha$ . The condition  $\Omega_{\mu\nu} u^\nu = 0$  then requires that  $l^\alpha$  be proportional to  $u^\alpha$ , i.e.,  $l^\alpha = \xi u^\alpha$ . One can then find the proportionality factor  $\xi$  in terms of  $\Omega^2$  to show (19) holds. With this relation, we have

$$\begin{aligned} \nabla_\mu J^\mu &= \rho^{-\frac{2}{3}} \left\{ \Omega^2 \left[ \Theta - \frac{2}{3\beta} u^\mu \partial_\mu \rho \right] + u^\mu \partial_\mu \Omega^2 \right\} \\ &= 2\rho^{-\frac{2}{3}} \left\{ \Theta \Omega^2 + \Omega^{\alpha\beta} u^\mu \nabla_\mu \Omega_{\alpha\beta} \right\} \\ &= 2\rho^{-\frac{2}{3}} \left\{ \Theta \Omega^2 - 2\Omega^{\mu\alpha} \Omega_{\mu\beta} (\nabla_\alpha u^\beta) \right\} = 0. \end{aligned}$$

Here we have used (14) in the second line and (18) in the third line, while the final vanishing follows from (19). Therefore, the enstrophy,

$$Z \equiv \int_{S^2} \rho^{-2/3} \Omega^2 u^0 d\Sigma = \int_{S^2} (\omega_{\mu\nu} \omega^{\mu\nu} + \frac{1}{2} a_\mu a^\mu) \gamma d\Sigma \quad (20)$$

is conserved, where the first term in the expression is just the vorticity two-form squared (as expected from the non-relativistic version), and the second one, which involves the acceleration  $a_\mu \equiv u^\nu \nabla_\nu u_\mu$ , accounts for the fact that the fluid world-lines are not necessarily geodesics. One important point to emphasize from (20) is that the factors of  $\rho$  cancel out in the end, so that the final expression for the enstrophy is independent of the energy density.

#### D. Numerical approach and setup

Our goal is to study the dynamical behaviour of a perturbed, otherwise stationary, fluid configuration dual to

the Kerr/Schwarzschild black hole in global  $AdS_4$  or the Poincaré patch. We next describe the different components of our numerical implementation.

### 1. Initial Data

Initial data for perturbations of the stationary fluid configurations are directly added to the fluid velocity such that eddys are induced. This is straightforwardly achieved by considering perturbations which, in the co-moving frame of the fluid, describe space varying velocities that change sign in a smooth manner along some particular direction chosen. In the case of the torus, this is straightforward as described in the appendix. For the spherical case, we adopt a perturbation in the fluid velocity as:

$$u^\phi \rightarrow u^\phi = \gamma \omega \equiv \gamma(\omega_0 + \delta\omega_p(\theta, \phi)), \quad (21)$$

for some small value  $\delta$  and a function  $\omega_p$  defined on the sphere (generally chosen to be one of the spherical harmonic basis functions  $Y_\ell^m(\theta, \phi)$ ). In this expression,  $\gamma$  is the local Lorentz factor defined for the full angular velocity  $\omega$ , including the  $\omega_p$  contribution. For future reference, it is useful to indicate the initial vorticity density associated to this flow,

$$\begin{aligned} W^0(\theta) &= \frac{1}{\sqrt{h}} \partial_\theta u_\phi = \frac{1}{\sin(\theta)} \partial_\theta [\sin^2(\theta) \gamma(\omega_0 + \delta\omega_p(\theta, \phi))] \\ &= (\omega_0 + \delta\omega_p) \gamma^3 \cos(\theta) (2 - \omega^2 \sin^2(\theta)) \\ &\quad + \delta\gamma^3 \sin(\theta) \partial_\theta \omega_p. \end{aligned}$$

From this expression, we see that the rigid rotation component (6) of the flow introduces a  $Y_1^0$  component to the vorticity at order  $\omega_0$  and higher  $\ell$  contributions also appear at higher orders in  $\omega_0$ . Thus for sufficiently fast flows, the background contribution renders analyzing turbulent behaviour through vorticity more delicate.

### 2. Grid Scheme

We now discuss details of our grid implementation and results. Since the qualitative behaviour is the same in both topologies considered –but the implementation is more involved in the spherical case– from now on we concentrate on the spherical flows to simplify the presentation and defer details of the toroidal case to the appendix.

Since the topology of our computational domain is  $S^2$ , we employ multiple patches to cover it in a smooth way. A convenient set of patches is defined by the *cubed sphere coordinates*. There are six patches with coordinates projected from the sphere, and each of this patches constitute a uniform grid — see figure 1). These grids are defined in a way such that there is no overlap and only grid points at boundaries are common to different grids

(*multi-block approach*). To ensure a correct transfer of information among the different grids we follow the technique described in [39], which relies on the addition of suitable *penalty terms* to the evolution equations to preserve the energy norm through the whole sphere. This technique ‘penalize’ possible mismatches between values the characteristic fields take at interfaces and enforce consistency through suitably introduced driving terms. Here we follow the strategy introduced in [40] which is an extension of the method introduced in [41, 42].

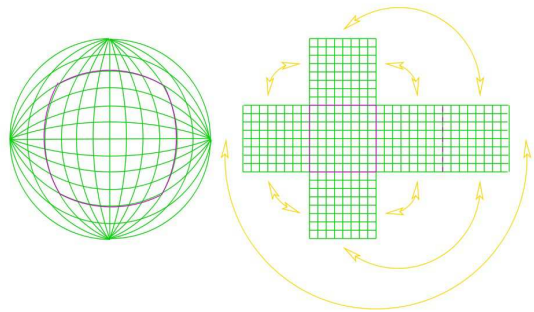


FIG. 1: *Cubed Sphere Coordinates*. A total of six Cartesian patches are employed to cover the sphere. Only patch boundaries coincide at common points.

Introducing coordinates  $\{t, x, y\}$  with  $(x, y)$  to label points in each Cartesian patch, the metric in each one reads,

$$ds^2 = -dt^2 + \frac{1}{D^2} \{ (1 + y^2) dx^2 + (1 + x^2) dy^2 - 2xy dx dy \}$$

where  $D \equiv 1 + x^2 + y^2$ . The non-vanishing Christoffel’s symbols are given by,

$$\Gamma_{xx}^x = \frac{-2x}{D}, \quad \Gamma_{xy}^x = \frac{-y}{D}, \quad \Gamma_{yy}^y = \frac{-2y}{D}, \quad \Gamma_{xy}^y = \frac{-x}{D}$$

### 3. Numerical Scheme and Stability

In order to construct stable finite difference schemes for our initial value problem we use the method of lines [34]. This means that we first discretize the spatial derivatives (constructing some suitable finite difference operators) and obtain a system of ordinary differential equations for the grid functions. To ensure the stability of the numerical scheme we use the *energy method* described on [35]. We employ (fourth/second-order accurate at interior/boundary points) finite difference operators satisfying *summation by parts* (the discrete analogue of integration by parts) and deal with interface boundaries with appropriate penalty terms at the interfaces as described in [39]. For the time integration, we adopt a 4<sup>th</sup> order Runge-Kutta algorithm.

All simulations were performed using 81x81 grids for each of the six patches, giving a total number of around

40.000 grid points to cover the entire sphere. We have confirmed convergence through several tests, in particular we adopted different initial data, and studied the numerical solutions with increased resolution with each grid having 321x321, 161x161, 81x81 points (labeled by 4,2,1 respectively). With each obtained solution, denoted by  $U^{(i)}(t, \theta, \phi)$  (for  $i = 4, 2, 1$ ), we calculated the *convergence rate*  $p$  as,  $Q(t) \equiv \frac{\|U^{(4)} - U^{(2)}\|_{L_2}}{\|U^{(2)} - U^{(1)}\|_{L_2}} \approx 2^p$ . For the cases considered, the obtained rate was in very good agreement with the expected for resulting 3<sup>rd</sup> order implementation constructed.

### III. RESULTS

We analyze the dynamics of small perturbations around the stationary fluid configurations duals to Schwarzschild and Kerr geometries on  $AdS_4$ . We separately study these two cases, starting with a qualitative description of the system evolutions, for generic perturbations. We show in figures 4 and 6 the sequence on the evolution of the vorticity field for the two cases. Then, in order to gain some insight into the turbulent behaviour and to capture the possible cascading phenomena, we perform a spherical harmonic decomposition (up to  $\ell=12$ ) of the relevant fields and compute their associated power spectrum as a function of time.

This signal processing analysis is derived simply from a generalization of *Parseval's theorem*, which states that the total power of a function  $f$  defined on the unit sphere is related to its spectral coefficients by,

$$\frac{1}{4\pi} \int_{S^2} |f(\theta, \phi)|^2 d\Sigma = \sum_{\ell=0}^{\infty} C_f(\ell),$$

$$C_f(\ell) = \sum_{m=-\ell}^{\ell} |A_{\ell m}|^2;$$

where  $A_{\ell m}$  are the coefficients of the expansion of  $f$  in the spherical harmonics. In figures 4 and 8, we plot the coefficients  $C(\ell)$  as a function of time, to analyze how the different modes behave during the evolution.

#### A. Non-rotating case: perturbations to Schwarzschild

One can basically classify the dynamical behaviour of the system into four different stages. In figure 2, we plot the vorticity field of a representative example for each one of them. A first stage corresponds to an initial transient period when the initial configuration seemingly remains unchanged for some time interval. (This interval depends on the perturbation considered, being shorter for larger  $\ell$ 's perturbations at a fixed value of  $\delta$ , but it does not

depend on the system's temperature). Closer inspection however reveals that non-trivial dynamics begins to manifest and an exponential growth of some modes sets in (see fig. 4). Notice that the initial growth rate of these modes is approximately the same though the higher  $\ell$ 's grow to larger values earlier. Since truncation errors feed higher frequencies this behaviour is not surprising. As these modes become large enough (roughly commensurate to the magnitude of the initial perturbation), the original symmetry of the system gets broken and a number of *eddies* arise and move around. Such an instant might be regarded as the beginning of turbulence (fig. 2(b)). As the dynamics continues, the eddies gradually turn into individual vortices and exhibit a seemingly chaotic motion, during a stage that we will refer as *fully developed turbulence* (fig. 2(c)). With the vortices propagating around the sphere, encounters of same-sign vortices lead to increasingly larger vortex structures. During this stage, governed by non-linear effects, energy transfers from the higher  $l$  modes to lower ones. The process continues until four vortices, two of each sign, are formed (fig. 2(d)).

The *end-state* is found to be qualitatively the same in all the cases we have considered, regardless of the initial perturbation introduced and of the system's temperature. We have explored generic perturbations in the velocity initial data, as described on (21): from different single-mode perturbations (i.e.,  $\omega_p \sim Y_{\ell}^m(\theta, \phi)$  for particular  $\ell$  and  $m$ ), to a random combination of all of them up to  $\ell = 12$ . We have further considered the inclusion of a random forcing term in the evolution equations, by adding a term  $f^\nu$  to the right hand side of the stress conservation equation as:  $\nabla_\mu T^{\mu\nu} = f^\nu$ . This force is given by a random field, both in time and space (and thus, acting on very short scales). Even in this forced case, the dynamical character and properties of the solution remain qualitatively unchanged. This (in addition to convergence studies) indicates that our grid structure is playing no significant role on the obtained behaviour and on the final configuration attained.

Main features of the long-term behaviour of the solution are illustrated in figure 3. In particular, the mentioned four dominant vortices of the resulting configuration. It can be noted that the temperature and energy densities attain local minimums at the vortices' locations and that the enstrophy is almost exclusively contained within them.

In figure 4 we have displayed a few representative modes of the vorticity power spectrum for an initial perturbation  $\omega_p(\theta, \phi) = Y_{10}^0(\theta, \phi)$ ,  $\delta = 0.2$  and  $\tau = 100$ . The coefficients  $C(\ell)$  of the spectrum are normalized with respect to the total power and plotted (in logarithmic scale) as a function of time. In the figure, the modes  $\ell = 9$  and  $\ell = 11$  dominate the spectrum at  $t = 0$  — as expected since the vorticity involves a derivative of the three-velocity and the initial data for the latter has a single  $\ell = 10$  mode. The rest of the modes exhibit an exponential growth on the early stages of the evolu-

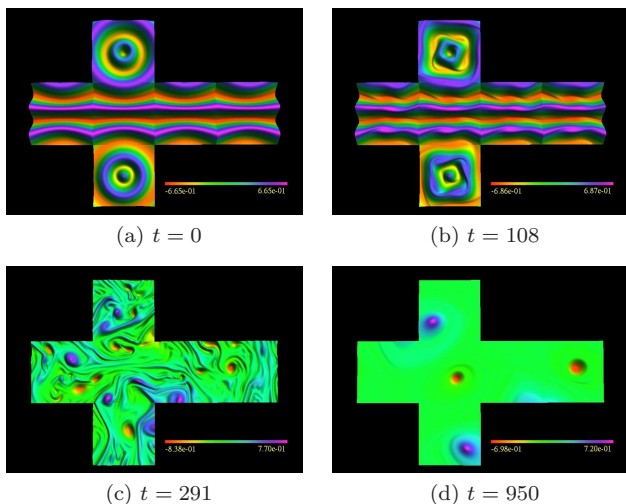


FIG. 2: Evolution of the vorticity field for a perturbation  $\omega_p(\theta, \phi) = Y_{10}^0(\theta, \phi)$  and  $\delta = 0.2$ , on Schwarzschild ( $\omega_0$ ). (a) Initial config., (b) beginning of turbulence, (c) *fully developed* turbulent stage, (d) final state.

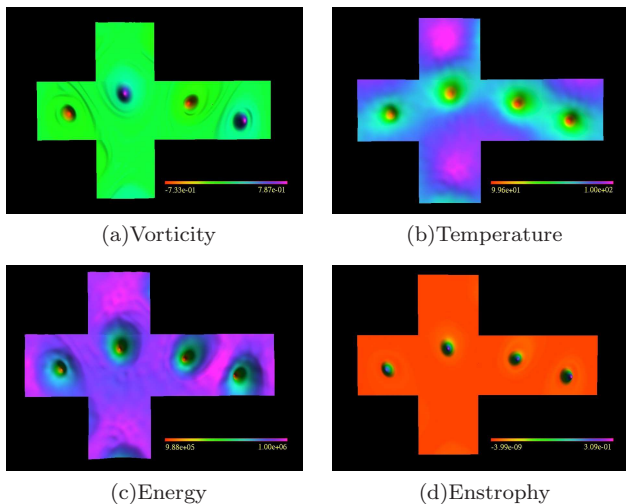


FIG. 3: Late times configuration for distinct relevant fields in the non-rotating case ( $\omega_0 = 0$  and  $T \sim 100$ , at  $t = 1200$ ). Notice that vortices correspond to minima in the energy. This behaviour is expected as stable vortex structure require a larger surrounding pressure that prevents its dispersion.

tion, as previously described. As the turbulent cascade begin, and after a short stage in which the mode structure is rather complex, the original high- $\ell$  modes decrease while the lower ones increase and gradually dominate the flow. Particularly the  $\ell = 2$  mode in the spectrum, which represents the quadrupole contribution, is the dominant mode at late times.

Note that the vortices in figure 3, i.e., the  $\ell = 2$  mode above, are essentially quasi-stationary as we have neglected here the viscous (and higher) contributions which would certainly affect the very long-time behaviour of the solution. As we noted before, one might wonder whether

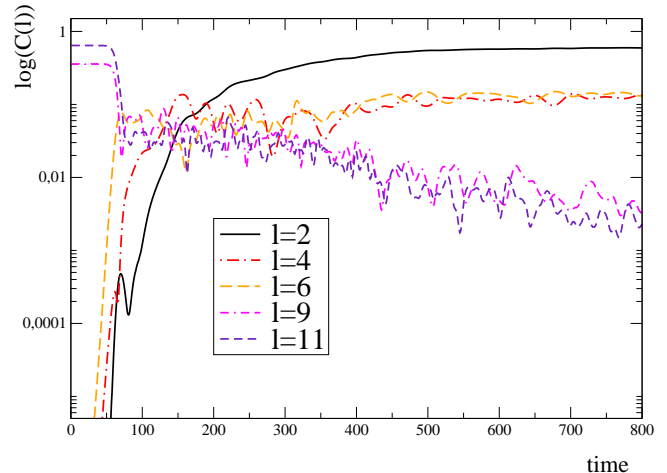


FIG. 4: Relevant modes in the power spectrum of the vorticity field for a  $\omega_p(\theta, \phi) = Y_{10}^0(\theta, \phi)$  and  $\delta = 0.2$  perturbation, in the non-rotating case (at temperature  $T \sim 100$ ).

the observed turbulent phenomena, and the conclusions we can draw from this study, might be significantly affected when such dissipative terms are taken into account. However, recall that in the discussion around (1), we argued the perfect fluid equations will give a good description when  $LT \gg 1$ . We verified the accuracy of this statement by comparing the system's dynamics at a variety of temperatures — recall that the radius of the sphere is fixed to be one — while keeping the initial data for  $u^k$  fixed. Figure 5 illustrates the behaviour of the  $L_2$  norm of  $u^\theta$ , i.e.,  $[\int_{S^2} |u^\theta|^2 d\Sigma]^{1/2}$ . The latter is a useful proxy for the solution's turbulent behaviour since in the absence of turbulence, it would remain zero by symmetry considerations. As is evident in this figure, the system's behaviour does not change as the temperature increases. In particular, the growth rate and both onset and full development of turbulence are essentially the same in all cases considered.

## B. Rotating case: perturbations to Kerr

The qualitative behaviour of the system on the rotating scenario is illustrated in figure 6, and it happens to be very similar to the presented above for the Schwarzschild case. However, we emphasize that these rotating solutions are not simply static solutions, i.e.,  $\omega_0 = 0$ , in a rotating frame. Recall that the rigid rotation introduces a background vorticity field, which one finds completely dominates the long-term behaviour. A key difference is evident immediately after the vortices are formed: the background rotation drags them into the main rotating stream and gradually separates them according to the direction of their rotation. If the background rotation flows

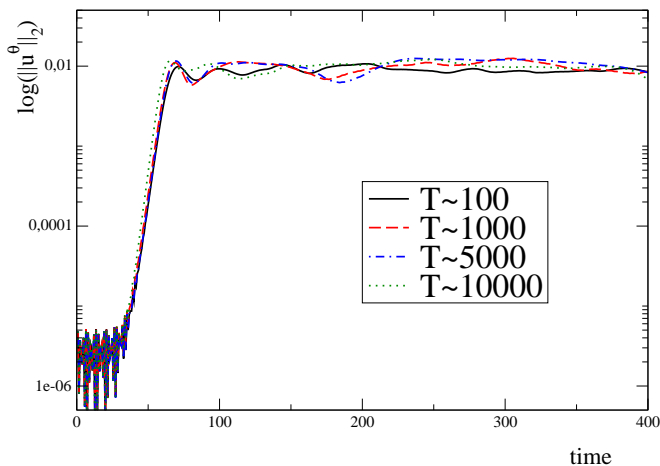


FIG. 5: Dependence with temperature: logarithm of the  $L_2$  norm of  $u^\theta$  for different temperatures, in the non-rotating case.

left to right as in fig. 6(c), clockwise rotating vortices accumulate in the southern (lower) hemisphere while the vortices with counter-clockwise rotation migrate towards the opposite pole. Then, the system undergoes a merging process (of co-rotating vortices) as in the non-rotating case, but now just one vortex of each sign remains at late times, as in fig. 6(d). The initial northwards/southwards propagation of counterclockwise/clockwise vortices can be also explained in terms of the equal-sign mergers of vortices by regarding each of the smaller vortices generated in the flow as interacting with two much larger vortices induced at the north and south pole by the rigid rotation component of the flow. Note that the ‘final’ two vortices are not necessarily in precise alignment with the rotation axis, being often the case that they remain orbiting around the poles.

Main features of the long-term behaviour of the solutions in the rotating scenario are illustrated in figure 7. In particular the mentioned two dominant vortices as they oscillate around the poles, with the temperature and energy attaining local minima at the vortices’ locations and being concentrated near the equator where the fluid velocity is larger. The enstrophy is again almost exclusively contained within the vortices.

In figure 8 we display representative modes of the vorticity spectra for two different parameters of the rotating solution with  $\tau = 100$  and a perturbation set by  $\omega_p(\theta, \phi) = Y_{10}^0(\theta, \phi)$  and  $\delta = 0.08$ . Here, the  $\ell = 1$  mode represents the background rotation contribution while the  $\ell = 9$  and  $\ell = 11$  modes are the ones associated with the perturbation, as discussed previously. We should recall here that the coefficients in the spectrum are normalized to unity, and thus it becomes clear from the plots that the long term dynamics is being completely dominated by the rotation.

For the case  $\omega_0 = 0.1$ , the configuration starts with

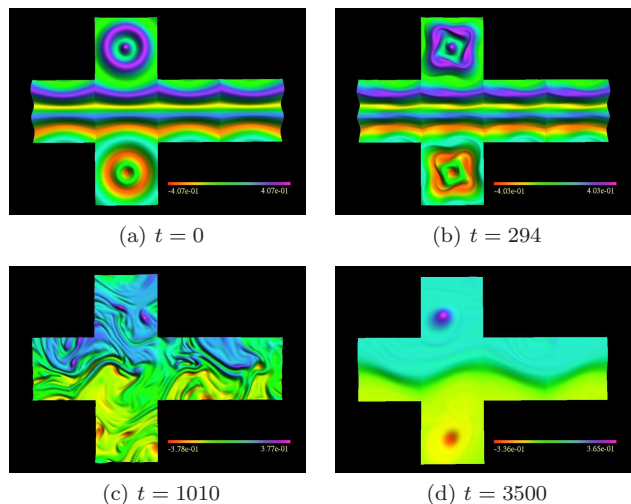


FIG. 6: Evolution of the vorticity field for a perturbation  $\omega_p(\theta, \phi) = Y_{10}^0(\theta, \phi)$  and  $\delta = 0.08$ , on a rigid rotation with  $\omega_0 = 0.1$ . (a) Initial config., (b) beginning of turbulence, (c) fully developed turbulent stage, (d) final state.

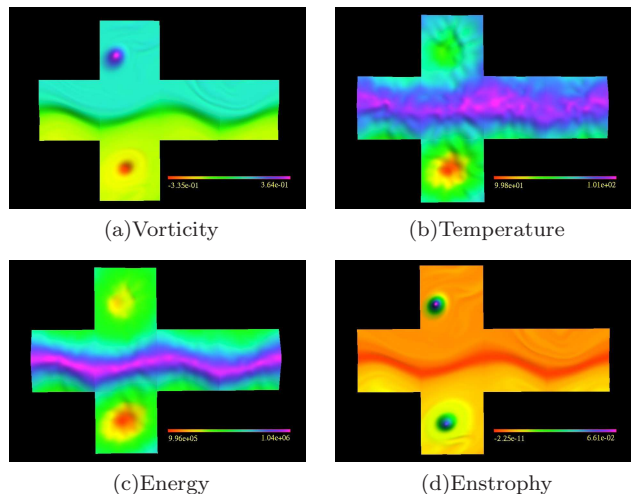


FIG. 7: The late time configuration for distinct relevant fields in the rotating case ( $\omega_0 = 0.1$  and  $T \sim 100$ , at  $t = 3600$ ).

a perturbation comparable in magnitude with the background motion. As the vortices form and turbulence begins, the high- $\ell$ ’s modes decrease displaying a cascading phenomena into lower  $\ell$  modes. In particular this cascade progresses towards the  $\ell = 1$  mode that eventually governs the state of the system. On top of this rotation dominated flow, the two vortical structures mentioned above persist and are represented in the spectrum by a combination of higher modes, predominantly the  $\ell = 2$  and  $\ell = 4$  modes.

Interestingly, for faster initial background rotations (i.e.,  $\omega_0 \gtrsim 0.5$ ) while keeping the perturbation amplitude  $\delta$  fixed, the flow is already dominated by the  $\ell = 1$  mode from the beginning and the turbulent stage takes longer to appear and fully develop. It seems that a strong



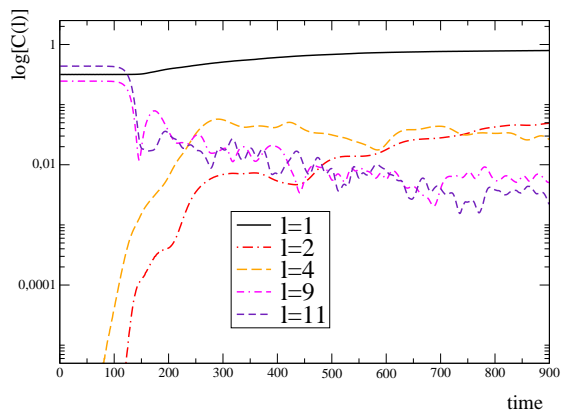
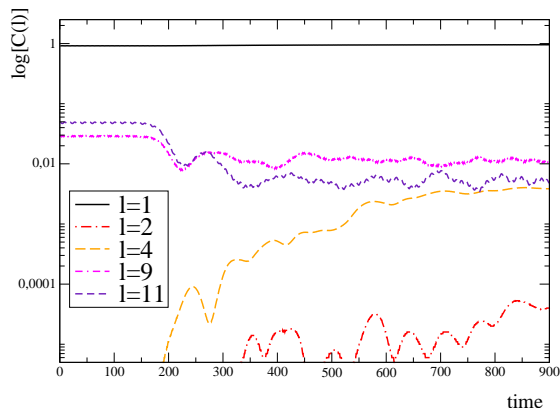
(a)  $\omega_0 = 0.1$ (b)  $\omega_0 = 0.5$ 

FIG. 8: Relevant modes in the power spectrum of the vorticity field in the rotating case (at temperature  $T \sim 100$ ), for two rotation parameters  $\omega_0$ . The initial perturbation is given by  $\omega_p(\theta, \phi) = Y_{10}^0(\theta, \phi)$  and  $\delta = 0.08$ .

rotating stream in the background hinders to a certain degree the formation and merging of vortices.

#### IV. DISCUSSION AND FINAL WORDS

In this work we have analyzed relativistic conformal fluid flows on both  $S^2$  and  $T^2$  backgrounds and found first that turbulence naturally arise in these flows and second that it gives rise to a ‘inverse’ cascade from shorter to longer wavelengths. These results not only extend common observations in Newtonian hydrodynamics but also have tantalizing implications for the behaviour of gravity in four-dimensional AdS spacetimes. Indeed, the AdS/CFT correspondence implies that for sufficiently high temperatures/length scales, the conformal fluid flows studied here have a dual description in terms of gravitational perturbations on Schwarzschild or Kerr black holes in AdS<sub>4</sub>, either with a spherical or planar horizon. The turbulent behaviour observed

here implies, through the duality, that gravitational perturbations in this limit should cascade to smaller frequencies. This constitutes a *prediction* obtained within holography which had not been previously anticipated on firm grounds[57]. Indeed, previously identified instabilities in AdS, *super-radiance* (e.g., [43]) and ‘*weak-turbulence*’[17, 45] imply a frequency shift towards higher frequencies. Therefore the cascading phenomena observed here implies an altogether new behaviour on the gravitational side. Furthermore, as described in [3, 5, 36], the full metric of the corresponding spacetime can be obtained and the implications of this cascading behaviour analyzed through suitable geometric quantities. We defer such tasks to a forthcoming work. We close noting that this possible cascade behaviour, first raised in [5] and demonstrated here (and presented in e.g., [46]) has now been observed in the Poincaré patch case [47].

Of course, another field theory ‘prediction’ is that large AdS black holes in five and higher dimensions will also exhibit turbulence but this chaotic behaviour will give rise to a ‘standard’ cascade to shorter wavelengths in these cases. From a gravitational perspective, this apparently generic behaviour for ‘hot’ horizons in AdS is completely unexpected and calls for a better understanding within gravity itself.

A step towards understanding the distinction between gravity in four and higher dimensions can be obtained by recalling that enstrophy conservation is what drives the hydrodynamics in 2+1 dimensions to exhibit the inverse cascade. One can then exploit the duality to translate the enstrophy into geometrical variables and to understand the implications of its conservation on the gravitational side. That is, the conservation of enstrophy in the fluid description implies a quasi-conserved quantity exists in the bulk gravity theory. Further, as we have seen here, the system displays a rich dynamical vortex configuration that merge towards a long lived state described by relatively few, long wavelength vortices. Isolated vortices in conformal fluids in 2+1 dimensions have been studied in [48] and their properties identified. Again using the fluid/gravity correspondence, one could produce a gravitational description of these quasi-stationary vortices. That the understanding of these or other geometrical quantities might help shed new light in turbulence phenomena is definitively an exciting prospect (see e.g., [49]).

Certainly, the full gravitational description will naturally incorporate dissipative contributions in the fluid flows. While we argued and quantitatively demonstrated that this dissipation will not modify the essential features of the turbulent behaviour at sufficiently high temperatures. In Newtonian hydrodynamics, the onset of turbulence is discussed in terms of the Reynolds number  $Re$ . The typical benchmark for the onset of turbulent flows is that  $Re$  have value of a few thousand. In relativistic hydrodynamics, the latter may be estimated as [50]

$$Re \sim \frac{TL}{\eta/s} = 4\pi TL, \quad (22)$$

where  $L$  is a characteristic length scale in the flow. In the last expression above, we have substituted the celebrated holographic value  $\eta/s = 1/4\pi$  [6, 7, 51] — we would have  $\eta/s = \beta$  for the general conformal fluid in (1). As this expression illustrates, we can produce arbitrarily large values of  $Re$  by increasing  $T$  (while keeping the system size fixed). Hence to observe turbulent behaviour, we are again naturally pushed to the regime where the hydrodynamic gradient expansion works well and our perfect fluid model becomes a good approximation. Of course, the viscous effects will definitely modify the very long-time behaviour observed here. For example, the conservation of the enstrophy is only true to first order in the hydrodynamic gradient expansion.

Of course, another interesting extension of the present investigation would be studying further the details of the turbulent cascade, in particular, the Kolmogorov scaling exponents. Figure 13 illustrates some preliminary results, which suggest that the ‘Newtonian’ kinetic energy will scale with the expected exponent of  $-5/3$ . However, various caveats must be noted. First, a clean easy-to-distinguish Kolmogorov-type reasoning applies to a situation where the turbulent flow is driven by an external force at some high frequency (in the present case of 2+1 dimensions) and viscous dissipation also damps the energy flow on much longer time scales. This scenario must be contrasted with the freely-decaying turbulence (i.e., without any driving force) which figure 13 describes. In freely-decaying turbulence determining the inertial range is more delicate but in such range (which shrinks as time proceeds) the  $-5/3$  slope can be distinguished. Additionally, Kolmogorov’s scaling arguments are made in a Newtonian context and can at best be regarded as approximate for the relativistic fluids studied here. Fortunately, the appropriate exact scaling relations applicable for relativistic hydrodynamic turbulence have been derived in [50]. The present simulations provide a framework for further studying these relativistic relations. More generally, however, the most exciting possibility would again be if a holographic perspective could provide new insights into the issues surrounding these turbulent cascades.

**Acknowledgments:** It is a pleasure to thank P. Chesler, R. Emparan, M. Kruczenski and T. Wiseman for interesting discussions. This work was supported by NSERC through Discovery Grants and CIFAR (to LL and RCM) and by CONICET, FONCYT and SeCyT-Univ. Nacional de Cordoba Grants (to FC and OR). F.C. thanks Perimeter Institute’s Visiting Graduate Fellows program for hosting his stay at the Perimeter Institute, where parts of this work were completed. Research at Perimeter Institute is supported through Industry Canada and by the Province of Ontario through the Ministry of Research & Innovation. Computations were performed at SciNet.

## Appendix A.

For comparison purposes, we also consider scenarios related to the dual case of an  $AdS_4$  black brane solution where the non-radial directions are compactified on a torus of size  $D$ . In Fefferman-Graham coordinates, labeled by  $(t, x, y)$ , the asymptotic metric is simply the flat one and the equations of motion can be straightforwardly implemented.

### A. Stationary solutions and initial data

Equilibrium configurations are given simply by constant flows at a given (arbitrary) temperature  $T$ . For simplicity we consider a torus with domain  $[0, D]^2$ . We then restrict to initial configurations with a flow along  $x$ , i.e.,  $u^a = \delta_x^a u_0$ , and introduce generic perturbations  $\delta u^a$  to this flow. For concreteness, we describe here two particular cases where the initial three-velocity is given by: case (A) with a perturbation of compact support,

$$u^a = \delta_x^a (u_0 + \delta u \sin(2\pi y/3) y^2 (y - L)^2) \quad (\text{A-1})$$

for  $0 \leq y \leq L$  and  $u^a = \delta_x^a u_0$  otherwise; and case (B)

$$u^a = \delta_x^a (u_0 + \delta u \sin(16\pi y/D)) . \quad (\text{A-2})$$

We note however the qualitative features observed in all cases considered remain the same.

### B. Turbulence, cascading behaviour and temperature dependence

We performed a series of numerical experiments adopting  $u_0 = 0, 0.1$  and  $0.5$  and  $\delta u = 0.01, \dots, 0.05$  (i.e., perturbations from 2% to 50%). and considered temperatures  $T \in [1, 10^3]$  with  $L = 10$  and typical grid sizes of  $[401, 401]$  (though consistency of behaviour was checked with grids 1.5 and 2 times better resolved).

As in the case of the sphere, the dynamics display a turbulent behaviour leading to the development of large vortices. As an illustrative example, Figure 9 displays the vorticity of the system at different times for case (A) with  $u_0 = 0.1$ ,  $\delta u = 0.01$  and  $T = 1$ . Early on, the behaviour is seemingly stationary but as turbulence develops the initial symmetry is completely broken and vortices arise which grow as they merger leading to a configuration described by long wavelengths.

As we have done in the  $S^2$  case we also study the system’s behaviour upon variation of temperature to ensure terms neglected in our study do not significantly affect the dynamics obtained. As in the previous case, a useful proxy to monitor the evolution is the  $(L_2)$  norm of  $u^y$  which, in the absence of turbulent dynamics, would remain zero. Figure 10 illustrates that the observed behaviour is essentially unchanged with temperature.

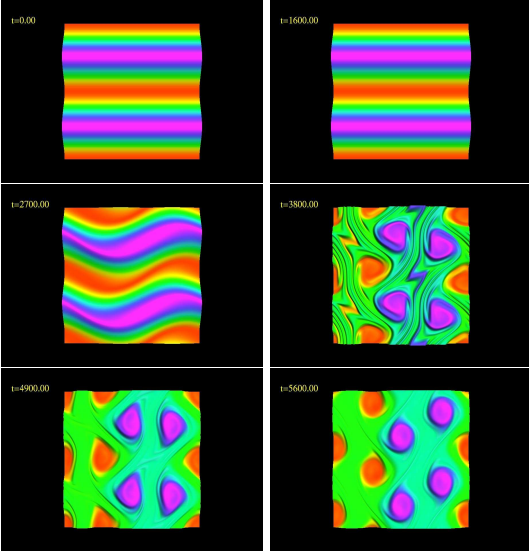


FIG. 9: Representative snapshots of the vorticity. As time progresses the initial configuration is strongly disturbed by the formation of vortices. As the dynamics continues, larger vortices are formed.

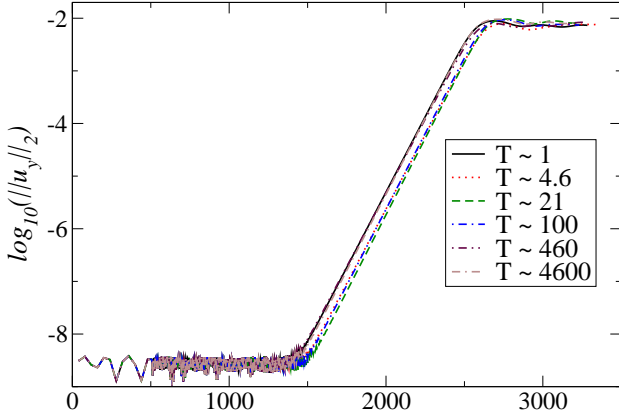


FIG. 10: Logarithm of the  $L_2$  norm of  $u^y$  for different temperatures. Essentially the behaviour observed is unchanged with temperature.

Last, we also considered varying the size of the torus by increasing  $D$  by factors of 1.5 and 2 in case (A) and

observed the same cascading behaviour.

To study how the energy cascades as time progresses, we compute the Fourier transform of energy density  $T^{00}$  and the vorticity density  $W^0$ . Since our computational grid is discretized by points  $\{x_i^1, x_j^2\}$  (with  $i, j = 1, \dots, N$ ), we denote  $\vec{n} = \{i, j\}$ , and write  $T^{00}(\vec{x}) = T^{00}(\vec{n})$  and the vorticity  $W^0(\vec{x}) = W^0(\vec{n})$ . The Fourier transform of these quantities is given by

$$\hat{T}^{00}(\vec{K}) = \sum_{\vec{n}} e^{-2\pi i \vec{K} \cdot \frac{\vec{x}}{N}} T^{00}(\vec{n}), \quad (\text{A-3})$$

$$\hat{W}^0(\vec{K}) = \sum_{\vec{n}} e^{-2\pi i \vec{K} \cdot \frac{\vec{x}}{N}} W^0(\vec{n}). \quad (\text{A-4})$$

Here  $\vec{K} = \{K_1, K_2\}$  and  $K_1, K_2 \in [0, N - 1]$ . Clearly,  $\hat{T}^{00}(\vec{K})$  and  $\hat{W}^0(\vec{K})$  are also represented on a  $N \times N$  grid. It is convenient to re-express the transformed quantities as functions of  $K = |\vec{K}|$ . From the functions  $\hat{T}^{00}(\vec{K})$  and  $\hat{W}^0(\vec{K})$ , we define  $T^{00}(K)$  and  $W^0(K)$  as follows

$$T^{00}(K) = \sum_i |T^{00}(\vec{K}_i)|, \quad (\text{A-5})$$

$$W^0(K) = \sum_i |W^0(\vec{K}_i)|, \quad (\text{A-6})$$

where the sums run over  $\vec{K}_i$ 's satisfying  $K \leq |\vec{K}_i| < K + 1$ . With this approach an effective wave-number grid of length  $\sqrt{2}N$  is obtained. Figure 11 illustrates a clear cascade to lower wave-numbers as time proceeds. In the case of  $T^{00}(K)$  the dominant mode is given by  $K = 1$  while for the vorticity both  $K = 1$  and  $K = 2$  are of similar magnitude. As in the  $S^2$  case, this is expected as the vorticity field is obtained by taking a single derivative which increases the mode content by one.

It is interesting to monitor whether the observed behaviour is consistent with the 'standard' Kolmogorov expectation. To illustrate this, we compute the Fourier transform of the 'Newtonian' kinetic energy per unit mass  $E = 1/2v^2$ . To make sense of this limit within our relativistic description, we chose  $u_0 = 0$  and  $\delta u = 0.03$ , whose solution is such that  $|v|$  is bounded by  $\simeq 0.04$  for all times, thus the fluid's motion stays far from relativistic speeds. Figure 12 shows the vorticity behaviour for this case and 13 illustrates the Fourier transformation of this kinetic energy for representative times. As time proceeds the energy in higher frequency modes diminishes while the opposite behaviour is observed for the lower ones. Additionally, at intermediate frequencies, the energy exhibits a behaviour with frequency consistent with a slope of  $-5/3$ , the expected Kolmogorov exponent.

[1] Juan Martin Maldacena. The Large N limit of superconformal field theories and supergravity. *Adv.Theor.Math.Phys.*, 2:231–252, 1998.

[2] Ofer Aharony, Steven S. Gubser, Juan Martin Maldacena, Hirosi Ooguri, and Yaron Oz. Large N field theories, string theory and gravity. *Phys.Rept.*, 323:183–386,

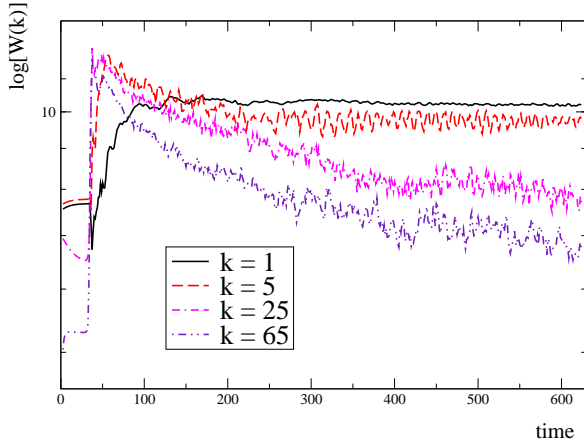
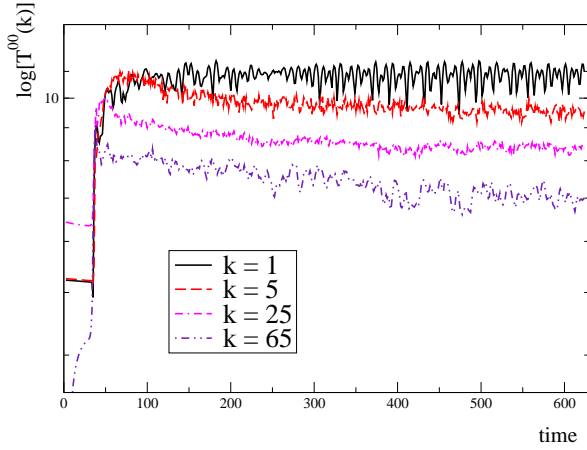


FIG. 11: Fourier modes for energy density (top panel) and vorticity density (bottom panel). As time progresses, a clear cascade to lower wave numbers is obtained.

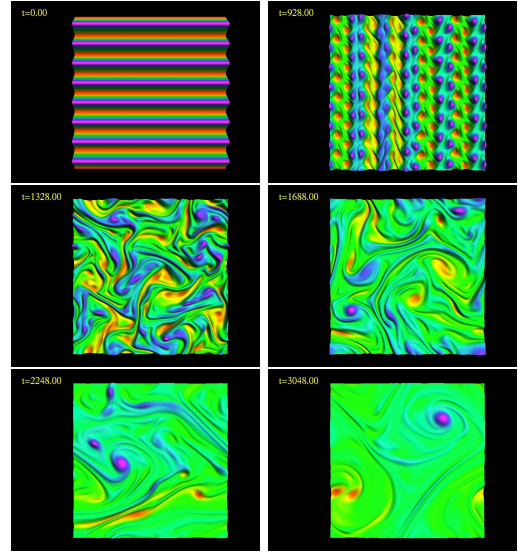


FIG. 12: Representative snapshots of the vorticity. Again, as time progresses a turbulent behaviour is clearly displayed and an apparent cascade to lower wavelengths.

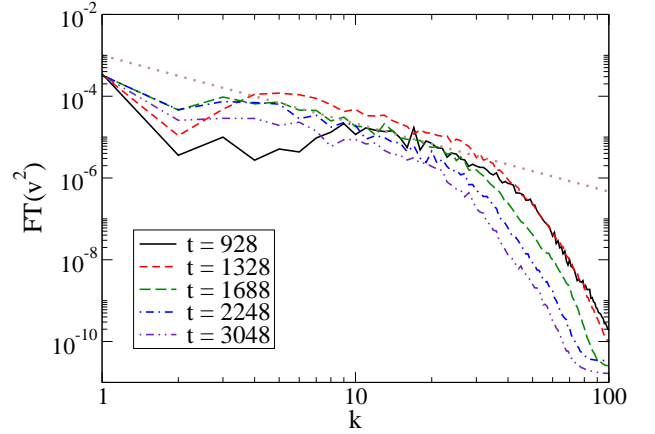


FIG. 13: Fourier modes for the kinetic energy density for representative times. As time progresses a cascading behaviour towards lower frequencies is manifested and in an intermediate ‘inertial regime’ with  $k \in (8, 400)$ , the scaling is quite consistent with a  $-5/3$  slope (indicated by a dotted line in the figure).

2000.

- [3] Sayantani Bhattacharyya, Veronika E Hubeny, Shiraz Minwalla, and Mukund Rangamani. Nonlinear Fluid Dynamics from Gravity. *JHEP*, 0802:045, 2008.
- [4] Sayantani Bhattacharyya, R. Loganayagam, Ipsita Mandal, Shiraz Minwalla, and Ankit Sharma. Conformal Nonlinear Fluid Dynamics from Gravity in Arbitrary Dimensions. Technical Report TIFR/TH/08-38, 2008.
- [5] Mark Van Raamsdonk. Black Hole Dynamics From Atmospheric Science. *JHEP*, 0805:106, 2008.
- [6] P. Kovtun, D.T. Son, and A.O. Starinets. Viscosity in strongly interacting quantum field theories from black hole physics. *Phys.Rev.Lett.*, 94:111601, 2005.
- [7] G. Policastro, D.T. Son, and A.O. Starinets. The Shear viscosity of strongly coupled  $N=4$  supersymmetric Yang-Mills plasma. *Phys.Rev.Lett.*, 87:081601, 2001.
- [8] Yaron Oz and Michael Rabinovich. The Penrose Inequality and the Fluid/Gravity Correspondence. *JHEP*,

1102:070, 2011.

- [9] Paul M. Chesler and Laurence G. Yaffe. Holography and colliding gravitational shock waves in asymptotically AdS5 spacetime. *Phys.Rev.Lett.*, 106:021601, 2011.
- [10] Keiju Murata, Shunichiro Kinoshita, and Norihiro Tanahashi. Non-equilibrium Condensation Process in a Holographic Superconductor. *JHEP*, 1007:050, 2010.
- [11] Simon Caron-Huot, Paul M. Chesler, and Derek Teaney.

- Fluctuation, dissipation, and thermalization in non-equilibrium AdS5 black hole geometries. *Phys.Rev.*, D84:026012, 2011.
- [12] David Garfinkle, Leopoldo A. Pando Zayas, and Dori Reichmann. On Field Theory Thermalization from Gravitational Collapse. *JHEP*, 1202:119, 2012.
- [13] Hans Bantilan, Frans Pretorius, and Steven S. Gubser. Simulation of Asymptotically AdS5 Spacetimes with a Generalized Harmonic Evolution Scheme. *Phys.Rev.*, D85:084038, 2012.
- [14] Alex Buchel, Luis Lehner, and Robert C. Myers. Thermal quenches in  $N=2^*$  plasmas. 2012.
- [15] Mariano Chernicoff, Daniel Fernandez, David Mateos, and Diego Trancanelli. Jet quenching in a strongly coupled anisotropic plasma. 2012.
- [16] C.-k. Chan, D. Mitra, and A. Brandenburg. Dynamics of saturated energy condensation in two-dimensional turbulence. *Phys. Rev. E*, 85(3):036315, March 2012.
- [17] Piotr Bizon and Andrzej Rostworowski. On weakly turbulent instability of anti-de Sitter space. *Phys.Rev.Lett.*, 107:031102, 2011.
- [18] Federico Carrasco, Luis Lehner, Robert Myers, Oscar Reula, and Ajay Singh. Conformal Fluids and Turbulent Behaviour in 2+1 Dimensions. Technical Report <http://spaces.perimeterinstitute.ca/2d-turbulence/content/2011-11-11>.
- [19] P.A. Davidson. *Turbulence: An Introduction for Scientists and Engineers*. Oxford University Press, USA, 2004.
- [20] Rose, H.A. and Sulem, P.L. Fully developed turbulence and statistical mechanics. *J. Phys. France*, 39(5):441–484, 1978.
- [21] Krzysztof Gawedzki. Easy turbulence. Technical Report IHES/P/99/56, August 1999.
- [22] R.H. Kraichnan. Inertial ranges in two-dimensional turbulence. *Phys. Fluids*, 10:1417–1423, 1967.
- [23] G.K. Batchelor. High Speed Computing in Fluid Dynamics. *Phys. Fluids*, 12:II–233, 1969.
- [24] James C. McWilliams. The emergence of isolated coherent vortices in turbulent flow. *Journal of Fluid Mechanics*, 146:21–43, 1984.
- [25] Vadim Borue. Inverse energy cascade in stationary two-dimensional homogeneous turbulence. *Phys. Rev. Lett.*, 72:1475–1478, Mar 1994.
- [26] R Benzi, G Paladin, S Patarnello, P Santangelo, and A Vulpiani. Intermittency and coherent structures in two-dimensional turbulence. *Journal of Physics A: Mathematical and General*, 19(18):3771, 1986.
- [27] Ingo Muller. Zum Paradoxon der Wärmeleitungstheorie. *Z.Phys.*, 198:329–344, 1967.
- [28] W. Israel and J.M. Stewart. Transient relativistic thermodynamics and kinetic theory. *Annals Phys.*, 118:341–372, 1979.
- [29] Robert Geroch and Lee Lindblom. Dissipative relativistic fluid theories of divergence type. *Phys. Rev. D*, 41:1855–1861, Mar 1990.
- [30] Robert Geroch and Lee Lindblom. Causal theories of dissipative relativistic fluids. *Annals of Physics*, 207(2):394–416, 1991.
- [31] Alex Buchel and Robert C. Myers. Causality of Holographic Hydrodynamics. *JHEP*, 0908:016, 2009.
- [32] Rudolf Baier, Paul Romatschke, Dam Thanh Son, Andrei O. Starinets, and Mikhail A. Stephanov. Relativistic viscous hydrodynamics, conformal invariance, and holography. *JHEP*, 0804:100, 2008.
- [33] Paul Romatschke. Relativistic Viscous Fluid Dynamics and Non-Equilibrium Entropy. *Class.Quant.Grav.*, 27:025006, 2010.
- [34] B. Gustafsson J. Olinger H. Kreiss. *Time Dependent Problems And Difference Methods*. John Wiley and Sons, Inc., 1995.
- [35] Gioel Calabrese, Luis Lehner, Oscar Reula, Olivier Sarbach, and Manuel Tiglio. Summation by parts and dissipation for domains with excised regions. Technical Report LSU-REL-080103, 2004.
- [36] Sayantani Bhattacharyya, Subhaneil Lahiri, R. Loganayagam, and Shiraz Minwalla. Large rotating AdS black holes from fluid mechanics. *JHEP*, 0809:054, 2008.
- [37] G.W. Gibbons, H. Lü, Don N. Page, and C.N. Pope. The general kerr–de sitter metrics in all dimensions. *Journal of Geometry and Physics*, 53(1):49–73, 2005.
- [38] Brandon Carter. Covariant theory of conductivity in ideal fluid or solid media. *Lecture Notes in Mathematics*, 1385:1–64, 1989.
- [39] Luis Lehner, Oscar Reula, and Manuel Tiglio. Multi-block simulations in general relativity: high order discretizations, numerical stability, and applications. *Class.Quant.Grav.*, 22:5283–5322, 2005.
- [40] Florencia Parisi and Oscar Reula. in preparation. 2012.
- [41] Mark H. Carpenter, Jan Nordström, and David Gottlieb. A Stable and Conservative Interface Treatment of Arbitrary Spatial Accuracy. *Journal of Computational Physics*, 148(2):341–365, 1999.
- [42] Jan Nordström and Mark H. Carpenter. High-Order Finite Difference Methods, Multidimensional Linear Problems, and Curvilinear Coordinates. *Journal of Computational Physics*, 173(1):149–174, 2001.
- [43] Elizabeth Winstanley. On classical superradiance in Kerr-Newman - anti-de Sitter black holes. *Phys.Rev.*, D64:104010, 2001.
- [44] J. Evslin, Hydrodynamic Vortices and their Gravity Duals. *Fortsch. Phys.* 60:1005, 2012. [arXiv:1201.6442 [hep-th]].
- [45] Oscar J.C. Dias, Gary T. Horowitz, and Jorge E. Santos. Gravitational Turbulent Instability of Anti-de Sitter Space. *Class.Quant.Grav.*, 29:194002, 2012.
- [46] Federico Carrasco, Luis Lehner, Robert Myers, Oscar Reula, and Ajay Singh. Conformal Fluids and Turbulent Behaviour in 2+1 Dimensions. Technical Report <http://pirsa.org/12060025/>, 2012.
- [47] Paul Chesler. in progress. 2012.
- [48] Jarah Evslin and Chethan Krishnan. Vortices in (2+1)d Conformal Fluids. *JHEP*, 1010:028, 2010.
- [49] Christopher Eling, Itzhak Fouxon, and Yaron Oz. Gravity and a Geometrization of Turbulence: An Intriguing Correspondence. 2010.
- [50] Itzhak Fouxon and Yaron Oz. Exact Scaling Relations In Relativistic Hydrodynamic Turbulence. *Phys.Lett.*, B694:261–264, 2010.
- [51] Christopher P. Herzog. The Hydrodynamics of M theory. *JHEP*, 0212:026, 2002.
- [52] Xiao Liu and Yaron Oz. Shocks and Universal Statistics in (1+1)-Dimensional Relativistic Turbulence. *JHEP*, 1103:006, 2011.
- [53] Irene Bredberg, Cynthia Keeler, Vyacheslav Lysov, and Andrew Strominger. From Navier-Stokes To Einstein. *JHEP*, 1207:146, 2012.
- [54] The one dimensional case has been studied in [52].
- [55] This issue does not arise in the Newtonian context and

a holographic scenario realizing this limit has been discussed in [53]. Consequently, the well known turbulent behaviour of Newtonian fluids is obtained in this case.

[56] Here, we have dropped the constant  $\alpha$  appearing in (1), which gives an overall normalization factor in the energy

density. Including this factor would simply produce an inconsequential constant shift of  $\tilde{\rho}$ .

[57] Note however the possibility had been raised earlier in [5, 44]